*Eurj*Chem **Eur**opean **J**ournal of **Chem**istry

APH ATLANTA PUBLISHING HOUSE

Coumarin-hydrazone-based fluorescence sensor for Al(III) detection in aqueous solution: DFT calculation and DNA interaction studies

Sunshine Dominic Kurbah [iD] 1,* and Ndege Simisi Clovis [iD] 2

1 Department of Chemistry, Pandit Deendayal Upadhyaya Adarsha Mahavidyalaya, Eraligool-788723, Karimganj, Assam, India
2 Department of Chemistry, Faculty of Science and Technology, University of Kinshasa, Kinshasa, Democratic Republic of Congo

* Corresponding author at: Department of Chemistry, Pandit Deendayal Upadhyaya Adarsha Mahavidyalaya, Eraligool-788723, Karimganj, Assam, India.
 e-mail: sunshinekurbah@yahoo.com (S.D. Kurbah).

RESEARCH ARTICLE

ABSTRACT

A new 'turn on' fluorescence chemosensor derived from coumarin-based compounds was successfully synthesised. N'-(2-Oxo-2H-chromene-3-carbonyl)isonicotinohydrazide (H_2L) was characterised by different spectroscopic techniques such as IR, UV-vis, and NMR spectroscopy. The electronic structures of H_2L and Al@HL were calculated using the density functional theory method using Becke's three parameter Lee-Yang-Parr (B3LYP) exchange functional with the 6-31G+(d,p) basis set. The detection limit of H_2L for the Al (III) ion was found to be 2.6 μM, which is low enough to detect micromolar and is below the World Health Organisation guideline for drinking water.

1. Introduction

In recent years, the development of highly sensitive and selective chemosensors for the detection of metal ions and anions has been of special interest to many researchers [1-4]. Not only because of their importance in living systems, medicine, and the environment, but also because they play essential roles in biological, chemical, ecological, and endocrine systems [5-8]. These metal ions and anions are also related to diverse environmental issues and other health-related problems. Therefore, analyses of these metal ions and anions both qualitatively and quantitatively have received significant attention [9-11]. Among the various metal elements, aluminium is the most abundant metal and is also known for its widespread use in daily life [12,13]. It is commonly used in the production of storage/cooking utensils, aluminium foils, alloys, food additives, and in the pharmaceutical industry. It is abundantly found in nature and is the third most prevalent metallic element in the crust of the Earth [14,15].

However, recently it has been shown to have considerable toxicity in biological systems and is widely known as a neurotoxic agent [16]. In the human body, the presence of unregulated amounts of aluminium could adversely affect the central nervous system of humans and cause many diseases such as Alzheimer's disease, Parkinson's disease, impaired memory, amyotrophic lateral sclerosis, and dialysis encephalopathy [17,18]. Therefore, the use of aluminium in medicine such as antacids and other aluminium-based pharmaceuticals, food additives, bleached flour, cooking utensils, and in the paper industry makes it more vulnerable to exposure to the environment to the trivalent ionic form of Al (III), leading to contamination of drinking water [19,20]. The Al(III) ion can also enter our brain, placenta, and foetus through the iron binding protein which acts as a carrier. Hence, the concentration of Al(III) in our body should be maintained at < 2 mg/g [17]. In this regard, the Environmental Protection Agency, USA, has set the standard amount of Al(III) ion in drinking water at 50 ppm [21,22]. Therefore, to encourage the public health benefits, the World Health Organisation (WHO) has recommended that the maximum level of Al(III) ion conta-mination is 7.4 μM in drinking water [23].

Thus, developing an efficient chemosensor for the rapid and sensitive detection of Al (III) ions is vital to comply with these standards and has gained great scientific interest among analytical chemists [3,4]. Existing methods including atomic absorption spectrometry (AAS), graphite furnace atomic absorption spectrometry (GF-AAS), inductively coupled plasma mass spectroscopy (ICP-MS), inductively coupled plasma atomic
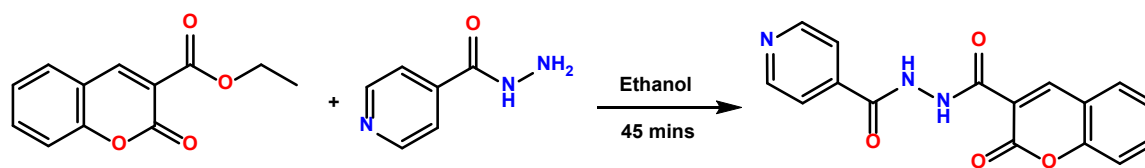
Scheme 1. The synthetic route of the compound H$_2$L.

emission spectrometry (ICP-AES), and electrochemical methods have been used for the detection of Al(III) ion [24,25]. Although these methods are sensitive, there are many limitations associated with them due to high cost, high background signals, and a tedious treatment of the sample. Therefore, the development of materials for a sensitive, selective, and effective detection method for Al(III) ion sensing is essential. Herein, we report a chemosensor for Al(III) ions based on coumarin with the desired properties for Al(III) ion analysis.

2. Experimental

2.1. Materials and instrumentation

The solvents were of reagent grade and were used as received. Other chemicals were E-Merck, Himedia, and equivalent grades, and all solvents were used as received. All operations were performed under aerobic conditions. C, H, and N were determined using a microanalytical method using the Perkin-Elmer 2400 CHN Analyser 11. Infrared spectra in the 4000-200 cm^{-1} range were recorded as KBr discs by using a BX-III/FTIR Perkin Elmer Spectrophotometer. ^{1}H NMR spectra were recorded on a Bruker Avance II 400 instrument in CDCl$_3$, solution using TMS as an internal standard. Electronic spectra were recorded on a Perkin-Elmer Lambda-25 spectrophotometer.

2.2. Synthesis of N'-(2-oxo-2H-chromene-3-carbonyl) isonicotinohydrazide (H$_2$L)

An ethanolic solution of ethyl coumarin carboxylate (0.22 g, 1 mmol) was added dropwise to a solution of isonicotinic hydrazide (0.14 g, 1 mmol) in ethanol under stirring conditions and the resulting solution was refluxed for 20 minutes and then stirred at room temperature for 1 hour. It afforded a white crystalline compound and dried under vacuum for further study (Scheme 1).

N'-(2-Oxo-2H-chromene-3-carbonyl)isonicotinohydrazide (H$_2$L): Color: White. Yield: 93%. M.p.: 193-211 °C. FT-IR (KBr, ν, cm^{-1}): 3417, 3271, 3059, 1678, 1592, 1530, 1478, 1342, 1281, 1150. ^{1}H NMR (400 MHz, CDCl$_3$, δ, ppm): 8.55 (s, 1H, NH$_a$), 7.68-7.62 (m, 4H, Ar-H), 7.38-7.33 (m, 4H, Ar-H), 7.29 (s, 1H, Ar-H), 5.06 (s, 1H, NH$_b$). ^{13}C NMR (100 MHz, CDCl$_3$, δ, ppm): 173, 168, 167, 155, 154, 143, 138, 130, 127, 124, 123, 122, 120, 118, 117, 28, 27. Anal. calcd. for C$_{16}$H$_{11}$N$_3$O$_4$: C, 62.14; H, 3.59; N, 13.59. Found C, 62.11; H, 3.62; N, 13.61%.

2.3. Fluorescence sensing study

Fluorescence detection experiments were performed using an aqueous ethanol-water solution (9:1, *v/v*) at room temperature. Fluorescence spectra were obtained with a Hitachi F-4500 spectrophotometer with quartz cuvette (path length = 1 cm). Fluorescence spectral measurements of water samples containing Al(III) were carried out by adding 15 ml of sensor H$_2$L (3 mM) and 0.60 ml of 50 mM bis-Tris buffer stock solution to 2.3 ml sample solution. After the mixture was mixed

for a few seconds, the fluorescence spectra were taken at room temperature.

2.4. DNA-binding studies

The DNA binding study experiments involving the binding of Al@HL with ct-DNA were performed by titration of the compounds with DNA and monitoring the changes spectroscopically. With a constant concentration of Al@HL (25 μM), the DNA concentration gradually increased (2.5-25.0 μM) and fluorescence titration was performed. The binding constant (K_a) for the Al@HL ensemble with ct-DNA was calculated using a Benesi-Hildebrand plot.

2.5. Computational studies

The electronic properties of the H$_2$L and Al@HL complex have been investigated by means of density functional theory (DFT) calculations. Theoretical studies were performed in the gas phase using density functional theory (DFT) with 6-31G+(d,p) basis sets implemented in the Gaussian09 programme.

2.6. Competition with other metal ions

The interaction between H$_2$L with different metal cations was investigated by fluorescence spectroscopy in aqueous ethanol-water solution (9: 1, v/v) at room temperature. The H$_2$L stock solution was prepared at a concentration of 1.0 mM and diluted to 50 mM. The fluorescence experiment was carried out by adding 1.3×10^{-4} M of different metal ions solutions, such as Zn^{2+}, Ni^{2+}, Cu^{2+}, Cd^{2+}, Hg^{2+}, Co^{2+}, Fe^{2+}, Ag^{2+}, Mg^{2+}, Cr^{3+}, Ca^{2+}, Na$^+$, K$^+$, Li$^+$, and Pb^{2+} to the H$_2$L solution (1.3×10^{-4} M). After the mixture was mixed for a few seconds, fluorescence spectra were obtained at room temperature.

3. Results and discussion

3.1. Synthesis and characterization

The H$_2$L probe was synthesised in good yield by simple reactions of ethyl coumarin carboxylate with isonicotinic hydrazide in a 1:1 molar ratio in ethanol solution (Scheme 1). H$_2$L was characterised by ^{1}H NMR spectroscopy. The H$_2$L shows a resonance at δ 8.55 and 5.06 ppm which are assigned to the NH_a and NH_b protons. The aromatic protons appeared at the expected position in the range of δ 7.29-7.68 ppm.

3.2. Fluorescence sensing study

The fluorescence detection study of Al@HL was evaluated using an ethanol-water mixture (9:1, *v/v*) by fluorescence spectral analysis at room temperature. As shown in Figure 1, H$_2$L excited at 405 nm shows very weak and broad emission in the range of 400 to 550 nm with a maximum wavelength at 465 nm.

The fluorescence experiment was carried out by adding 1.3×10^{-4} M of different metal ions, such as Zn^{2+}, Ni^{2+}, Cu^{2+}, Cd^{2+}, Hg^{2+}, Co^{2+}, Fe^{2+}, Ag^{2+}, Mg^{2+}, Cr^{3+}, Ca^{2+}, Na$^+$, K$^+$, Li$^+$, and Pb^{2+}. Upon the addition of these metal ions, the fluorescence intensity remains the same without enhancement, but upon addition
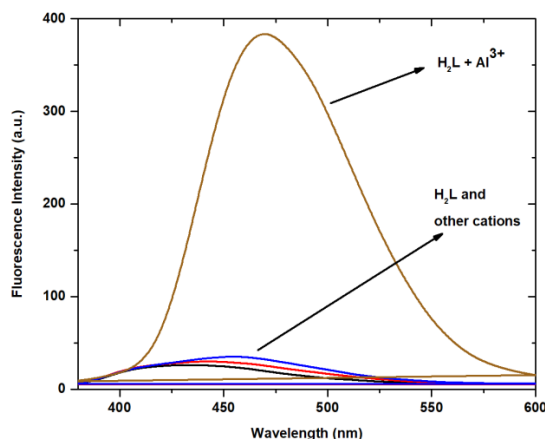
Figure 1. Fluorescence spectra of the complex after the addition of the Al(III) ion (2.0 equiv.) and other metal ions in ethanol/H₂O solution (v/v, 9:1).
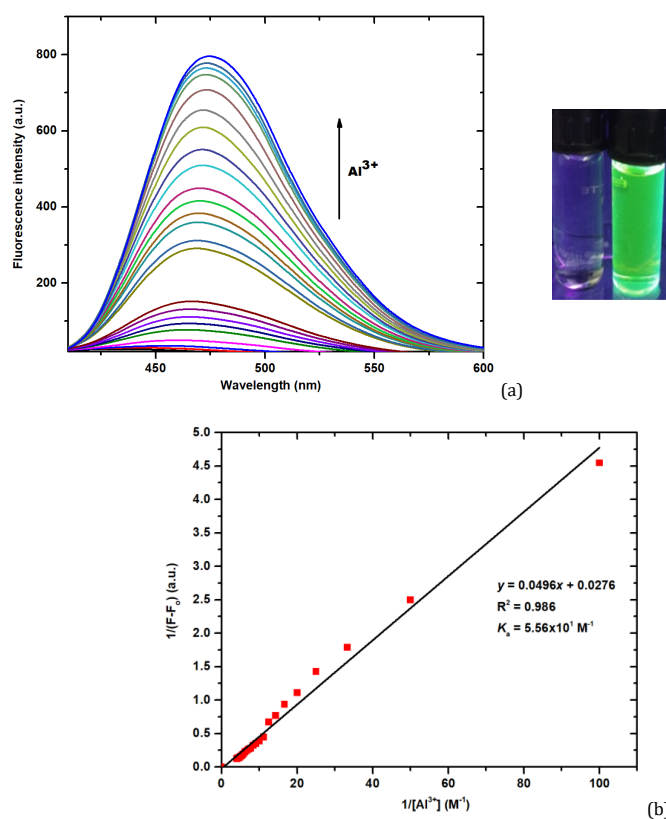

Figure 2. (a) Fluorescence spectral changes in the presence of 10-100 μM Al(III) ions in buffer solution and (b) Benesi-Hildebrand plot of fluorescence titration of H₂L with Al(III) ions.

3.5×10^{-4} M of the Al(III) ion resulted in a maximum increase in intensity as shown in Figure 1. Fluorescence enhancement was derived from the strong complexation of H₂L with the Al(III) ion, which inhibits C=N isomerisation and the photoinduced electron transfer process [26]. Fluorescence titration experiments were carried out by titrating H₂L with Al(III) ion (0.0-4.0 equiv.). However, the intensity of fluorescence emission of H₂L gradually increases with increasing concentration of the Al(III) ion, as shown in Figure 2.

The emission wavelength shows red-shifted to 475 nm upon the addition of 1 equivalent of Al(III) ion. These obtained results can be attributed to inhibition of the photoinduced electron transfer process after complexation of H₂L with the Al(III) ion, which significantly enhanced the fluorescence with a large red-shift change in emission wavelength. Furthermore,

from the above fluorescence titration profile, we have calculated the association constant of the Al@HL complex using the Benesi-Hildebrand plot and it was found to be 5.56×10^{1} M^{-1}. Therefore, the detection limits for Al(III) ions were calculated (Equation 1) and were found to be 2.75×10^{-6} M , which is sufficiently low to detect the micromolar. The results were comparable to some selective and sensitive fluorescent sensors reported in the literature and recognised the Al(III) ion in environmental and biological samples [27].

$$\text{Limit of detection (LOD)} = \frac{3.3 \times \sigma}{\text{Slope}} \qquad (1)$$

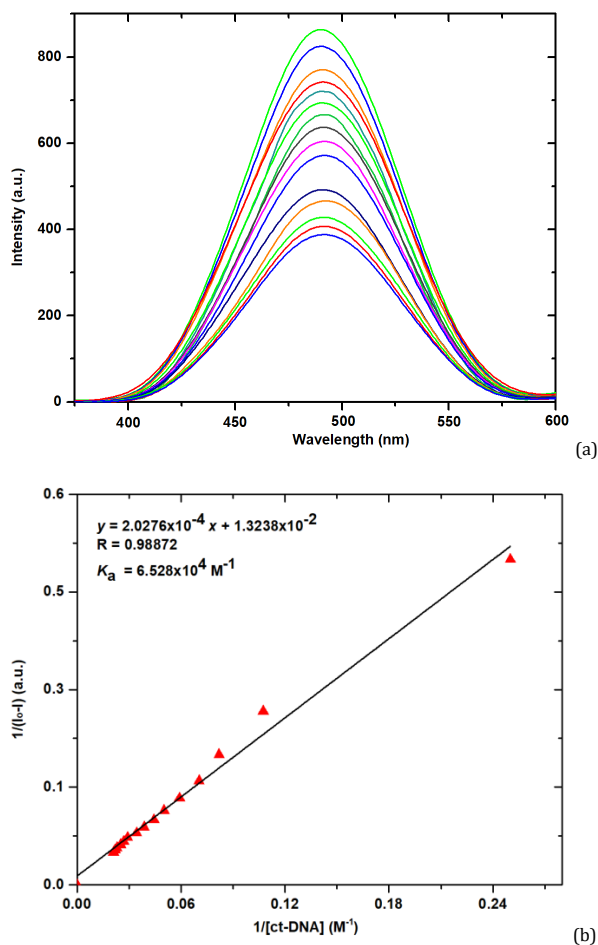σ is the standard deviation of the response.

Figure 3. (a) Fluorescence titration spectra of Al@HL with incremental addition of ct-DNA (0.0-2.0 equiv.) and (b) Benesi-Hildebrand plot of fluorescence titration of Al@HL with ct-DNA.

3.3. DNA binding studies

The binding studies of Al@HL complex with ct-DNA were studied using fluorescence spectroscopy. Metal complexes can bind to DNA by electrostatic interaction, groove binding, and intercalative binding [28]. The affinity of Al@HL toward ct-DNA was monitored by the change in emission intensity during fluorescence titration. As shown in Figure 3a, upon the addition of ct-DNA (0.0-2.0 equiv.), the solution of Al@HL decreases the fluorescence intensity of Al@HL, resulting in quenching of fluorescence. The quenching of fluorescence is probably due to the interaction of ct-DNA and the removal of the coordinated Al(III) ion from the Al@HL. The fluorescence intensity plot versus the concentration of ct-DNA at 475 nm shows good linearity, which allows quantitative detection of ct-DNA. The binding constant (K_a) for the Al@HL ensemble with ct-DNA was calculated using the Benesi-Hildebrand plot and was found to be 6.528×10^4 M^{-1} (Figure 3b).

To understand the complex binding behaviour of the H$_2$L and Al(III) ions, spectroscopic titration experiments were also performed using ^{1}H NMR spectroscopy. The experiment was carried out by adding 0.5-2.0 equivalents of the Al (III) ion to the solution of H$_2$L in the CDCl$_3$ solution. Upon the addition of 0.5 equivalent of Al(III) ion, the proton (NHb) decreases its intensity upon the addition of 0.5-2.0 equivalents of Al(III), as shown in Figure 4. These results suggested that the amine proton might interact strongly with the Al(III) ions, resulting in deprotonation. Similarly, there are also significant shifts in the aromatic protons. These results suggested that there is a strong binding

of the Al(III) ion with H$_2$L, resulting in the formation of a rigid complex through the oxygen and nitrogen donor atoms of the ligand.

3.4. Computational studies

To further evaluate the binding properties and geometry of the Al @ HL complex and the corresponding shift in the absorption spectra of H$_2$L-Al(III), we performed a calculation using density functional theory with the hybrid functional B3LYP and the 6-31G+(d,p) basis set [29-32]. The optimised geometries of H$_2$L and Al@HL are shown in Figure 5 and the bond lengths and bond angles are given in Tables 1 and 2.

The H$_2$L ligand binds to metal ions in a tridentate fashion through O19, N21, and O3 donor atoms. The metal ligand bond lengths are 1.957 Å (O3-Al34), 1.940 Å (O19-Al34), 1.974 Å (N21-Al34), 2.286 Å (Cl36-Al34), 2.283 Å (Cl37-Al34) and 1.99 Å (O35-Al34). The metal ligand bond angles are 87.32° (O3-Al34-N21), 80.80° (N21-Al34-O19), 168.11° (O3-Al34-O19), 96.92° (N21-Al34-Cl37), 83.21° (Cl37-Al34-O35), 177.63° (N21-Al34-O35) and 95.05° (O3-Al34-O35). As shown in Figure 5a, the ligand is involved in the intramolecular hydrogen bond interaction, with a bond distance of 1.98 Å.

The HOMO-LUMO orbitals of H$_2$L and Al@HL are shown in Figure 6. HOMO and LUMO analysis have been used to calculate the ionisation potential (IP), electron affinity (EA), electronegativity (χ), electrophilicity index (ω), hardness (η), chemical potential (μ), and first electron excitation (τ) are all correlated and given in Table 3.

Table 1. Bond lengths (Å) of H_2L and Al@HL.

H2L						Al@HL					
Atom	Atom	Bond length	Atom	Atom	Bond length	Atom	Atom	Bond length	Atom	Atom	Bond length
O3	C2	1.216	C12	O13	1.240	O3	C2	1.240	C14	N20	1.332
C2	O1	1.383	C12	N21	1.353	C2	O1	1.356	C14	O19	1.270
C2	C4	1.465	N20	N21	1.378	C2	C4	1.450	C14	C15	1.480
O1	C11	1.366	C14	N20	1.364	O1	C11	1.370	C15	C16	1.399
C10	C11	1.396	C14	O19	1.230	C10	C11	1.394	C16	C17	1.395
C9	C10	1.392	C14	C15	1.501	C9	C10	1.392	C17	N30	1.340
C8	C9	1.407	C15	C16	1.399	C8	C9	1.408	N30	C31	1.340
C7	C8	1.387	C16	C17	1.395	C7	C8	1.386	C18	C31	1.395
C6	C7	1.412	C17	N30	1.341	C6	C7	1.412	C15	C18	1.401
C5	C6	1.432	N30	C31	1.339	C6	C11	1.407	O3	Al34	1.957
C4	C5	1.363	C18	C31	1.397	C5	C6	1.429	N21	Al34	1.974
C6	C11	1.409	C15	C18	1.401	C4	C5	1.367	O19	Al34	1.940
C4	C12	1.495				C4	C12	1.499	O35	Al34	1.990
						C12	O13	1.245	Cl36	Al34	2.286
						C12	N21	1.345	Cl37	Al34	2.283
						N20	N21	1.378			

Table 2. Bond angles (°) of H_2L and Al@HL.

H2L							Al@HL						
Atom	Atom	Atom	Bond angles	Atom	Atom	Atom	Bond angles	Atom	Atom	Atom	Bond angles	Atom	Atom	Atom	Bond angles
O1	C2	O3	117.02	C4	C12	O13	121.89	O1	C2	O3	114.15	O19	C14	C15	121.11
O3	C2	C4	126.39	O13	C12	N21	121.01	O3	C2	C4	127.44	C14	C15	C16	118.42
C2	O1	C11	123.43	C12	N21	N20	117.37	C2	O1	C11	123.19	C15	C16	C17	118.52
C2	C4	C12	122.11	N21	N20	C14	119.27	C2	C4	C12	123.04	C16	C17	N30	123.75
C2	C4	C5	120.13	N20	C14	C15	115.86	C2	C4	C5	118.92	C17	N30	C31	117.26
O1	C11	C10	117.58	N20	C14	O19	121.20	O1	C11	C10	117.50	N30	C31	C18	123.74
O1	C11	C6	120.78	O19	C14	C15	122.94	O1	C11	C6	120.27	C15	C18	C31	118.50
C9	C10	C11	118.62	C14	C15	C16	117.74	C9	C10	C11	118.25	C16	C15	C18	118.23
C8	C9	C10	120.98	C15	C16	C17	118.73	C8	C9	C10	120.96	C14	C15	C18	123.35
C7	C8	C9	119.91	C16	C17	N30	123.74	C7	C8	C9	120.13	N21	Al34	O19	80.80
C6	C7	C8	120.33	C17	N30	C31	117.13	C6	C7	C8	120.20	N21	Al34	Cl37	96.92
C11	C6	C5	117.47	N30	C31	C18	123.76	C11	C6	C5	117.37	N21	Al34	Cl36	96.86
C5	C6	C7	124.02	C15	C18	C31	118.64	C5	C6	C7	124.39	N21	Al34	O3	87.32
C4	C5	C6	121.60	C16	C15	C18	118.00	C4	C5	C6	121.85	N21	Al34	O35	177.63
C5	C4	C12	117.76	C14	C15	C18	124.26	C5	C4	C12	118.04	O3	Al34	O19	168.11
								C4	C12	O13	120.63	O3	Al34	O35	95.05
								O13	C12	N21	124.10	O3	Al34	Cl37	88.92
								C12	N21	N20	113.29	O3	Al34	Cl36	88.76
								N21	N20	C14	115.92	Cl36	Al34	Cl37	165.90
								N20	C14	C15	120.72	Cl36	Al34	O35	83.14
								N20	C14	O19	118.17	Cl37	Al34	O35	83.21
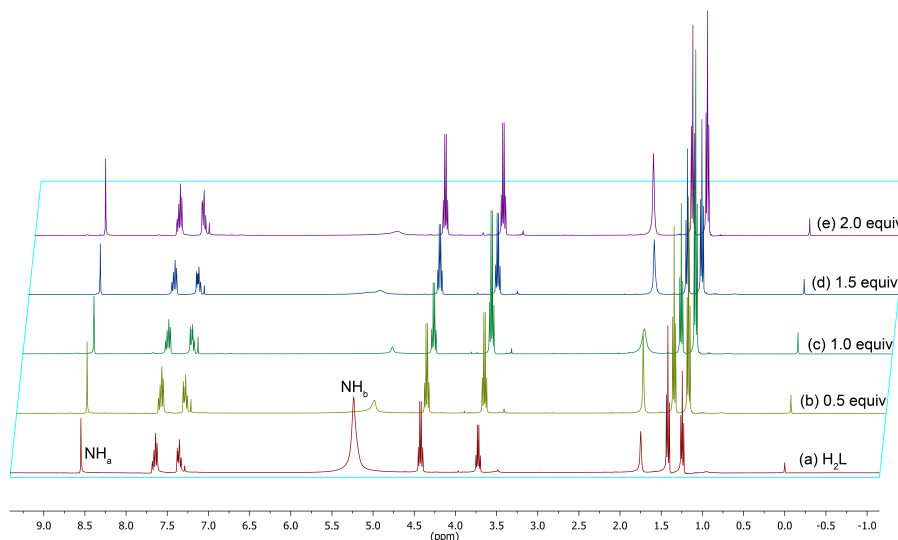
Figure 4. ^1H NMR spectra of (a) H_2L only and H_2L in the presence of (b) 0.5 equiv., (c) 1.0 equiv., (d) 1.5 equiv., and (e) 2.0 equiv. of Al(III) in $CDCl_3$.

Charges distribution analysis on individual atom obtained from NBO analysis for H_2L and Al@HL [32]. The charges on oxygen are -0.478 (O1), -0.559 (O3), -0.648 (O13) and -0.600 e (O19) while those of nitrogen are -0.446 (N20), -0.434 (N21) and -0.424 e (N30) in H_2L, whereas the charges of these atoms in Al@HL are -0.665 (O3), -0.446 (O1), -0.656 (O13), -0.713 (O19), -0.381 (N20), -0.586 (N21), -0.417 (N30) and 1.692 (Al34). As we have seen, upon the formation of an Al@HL complex, the charge increases slightly on the coordinated atom, giving rise to charge transfer to Al(III) in the complexation. The geometrical parameters obtained and the charge distribution were compared with the literature and are in good agreement [33,34].
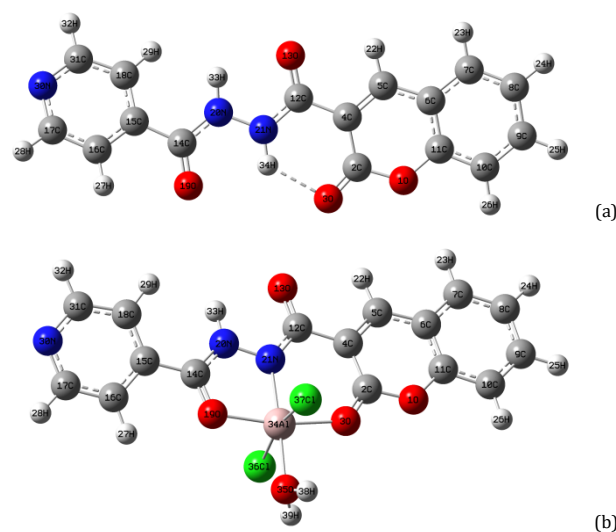
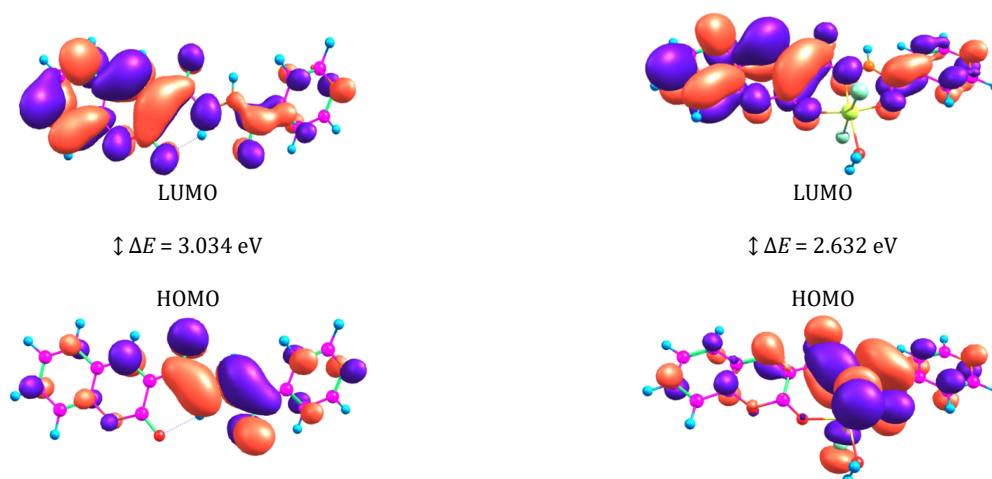**Figure 5.** (a) Optimised geometrical structure of H₂L and (b) Al@HL.

LUMO

$\updownarrow \Delta E = 3.034$ eV

HOMO

LUMO

$\updownarrow \Delta E = 2.632$ eV

HOMO

Figure 6. Energy level diagrams of HOMO and LUMO orbitals of H₂L and Al@HL complex calculated on the DFT level using a B3LYP method.

Table 3. Quantum chemical properties for H₂L and Al@HL.

Parameters	H₂L	Al@HL
Self-consistent field energy (a.u.)	-1081.547	-2320.464
Dipole moment (Debye)	7.224	7.527
LUMO energy (eV)	-2.933	-3.322
HOMO energy (eV)	-5.967	-5.954
Energy gap (eV)	3.034	2.632
Ionization potential (eV)	5.967	5.954
Electron affinity (eV)	2.933	3.322
Chemical hardness (eV)	1.517	1.316
Global softness (eV⁻¹)	0.330	0.380
Electronegativity (eV)	4.450	4.638
Chemical potential (eV)	-4.450	-4.638
Electrophilicity (eV)	6.527	8.173

4. Conclusion

We have designed and synthesised a simple fluorescent chemosensor derived from coumarine that can be used for the detection of Al(III) ions. The fluorescence sensing study of Al@HL was carried out using ethanol-water. The fluorescence spectrum of H₂L when excited at 405 nm shows very weak and broad emission. Moreover, upon addition of different metal ions, the fluorescence intensity shows no change, whereas upon addition of Al(III) ions resulted in a maximum increased in intensity. The fluorescence enhancement was derived from the strong complexation of H₂L with Al(III), inhibiting the C=N isomerisation and the photoinduced electron transfer process.

Disclosure statement DS

Conflict of interest: The authors declare that they have no conflict of interest.
Ethical approval: All ethical guidelines have been adhered.
Sample availability: Samples of the compounds are available from the author.

CRediT authorship contribution statement CR

Conceptualization: Sunshine Dominic Kurbah; Methodology: Sunshine Dominic Kurbah; Software: Sunshine Dominic Kurbah, Ndege Simisi Clovis; Validation: Sunshine Dominic Kurbah, Ndege Simisi Clovis; Formal Analysis: Sunshine Dominic Kurbah, Ndege Simisi Clovis; Investigation: Sunshine Dominic Kurbah, Ndege Simisi Clovis; Resources: Sunshine Dominic Kurbah, Ndege Simisi Clovis; Data Curation: Sunshine Dominic Kurbah, Ndege Simisi Clovis; Writing - Original Draft: Sunshine Dominic Kurbah, Ndege Simisi Clovis; Writing - Review and Editing: Sunshine Dominic Kurbah, Ndege Simisi Clovis; Visualization: Sunshine Dominic Kurbah, Ndege Simisi Clovis.

ORCID and Email

Sunshine Dominic Kurbah

 sunshinekurbah@yahoo.com

 https://orcid.org/0000-0001-5029-3815

Ndege Simisi Clovis

 ndgclo@gmail.com

 https://orcid.org/0000-0001-9161-3109

References

[1]. Smith, B. A.; Akers, W. J.; Leevy, W. M.; Lampkins, A. J.; Xiao, S.; Wolter, W.; Suckow, M. A.; Achilefu, S.; Smith, B. D. Optical imaging of mammary and prostate tumors in living animals using a synthetic near infrared zinc(II)-dipicolylamine probe for anionic cell surfaces. *J. Am. Chem. Soc.* **2010**, *132*, 67–69.

[2]. Nolan, E. M.; Racine, M. E.; Lippard, S. J. Selective Hg(II) detection in aqueous solution with thiol derivatized fluoresceins. *Inorg. Chem.* **2006**, *45*, 2742–2749.

[3]. Kamaci, Ü. D.; Kamaci, M. Boric acid and Schiff base-based fluorescent sensor for detection of L-tryptophan in milk and BSA samples. *Turk. J. Chem.* **2022**, *46*, 929–940.

[4]. Aydıner, B. Coumarin-based benzilmonohydrazone as a new proton-sensitive fluorescencedye: synthesis and investigation of photophysical and acidochromic properties. *Turk. J. Chem.* **2019**, *43*, 1086–1097.

[5]. Karakuş, E. An anthracene based fluorescent probe for the selective and sensitive detection of Chromium (III) ions in an aqueous medium and its practical application. *Turk. J. Chem.* **2020**, *44*, 941–949.

[6]. Hentze, M. W.; Muckenthaler, M. U.; Andrews, N. C. Balancing acts. *Cell* **2004**, *117*, 285–297.

[7]. Ma, Y.-R.; Niu, H.-Y.; Zhang, X.-L.; Cai, Y.-Q. Colorimetric detection of copper ions in tap water during the synthesis of silver/dopamine nanoparticles. *Chem. Commun. (Camb.)* **2011**, *47*, 12643–12645.

[8]. Ha, W.; Yu, J.; Wang, R.; Chen, J.; Shi, Y.-P. "Green" colorimetric assay for the selective detection of trivalent chromium based on Xanthoceras sorbifolia tannin attached to gold nanoparticles. *Anal. Methods* **2014**, *6*, 5720–5726.

[9]. Dixon, S. J.; Stockwell, B. R. The role of iron and reactive oxygen species in cell death. *Nat. Chem. Biol.* **2014**, *10*, 9–17.

[10]. Carter, K. P.; Young, A. M.; Palmer, A. E. Fluorescent sensors for measuring metal ions in living systems. *Chem. Rev.* **2014**, *114*, 4564–4601.

[11]. Ucuncu, M. A BODIPY based probe for the reversible "turn on" detection of Au(III) ions. *Turk. J. Chem.* **2022**, *46*, 523–529.

[12]. Sahana, A.; Banerjee, A.; Lohar, S.; Banik, A.; Mukhopadhyay, S. K.; Safin, D. A.; Babashkina, M. G.; Bolte, M.; Garcia, Y.; Das, D. FRET based tri-color emissive rhodamine-pyrene conjugate as an Al3+ selective colorimetric and fluorescence sensor for living cell imaging. *Dalton Trans.* **2013**, *42*, 13311–13314.

[13]. Goswami, S.; Paul, S.; Manna, A. Selective "naked eye" detection of Al(iii) and PPi in aqueous media on a rhodamine–isatin hybrid moiety. *RSC Adv.* **2013**, *3*, 10639.

[14]. Maimaiti, Y.; Maimaitiyiming, X. A highly selective and sensitive fluorescent turn-off probe for Al3+ based on polypyrimidine. *Fiber. Polym.* **2020**, *21*, 7–18.

[15]. Keawwangchai, T.; Morakot, N.; Wanno, B. Fluorescent sensors based on BODIPY derivatives for aluminium ion recognition: an experimental and theoretical study. *J. Mol. Model.* **2013**, *19*, 1435–1444.

[16]. Badugu, R. Fluorescence sensor design for transition metal ions: the role of the PIET interaction efficiency. *J. Fluoresc.* **2005**, *15*, 71–83.

[17]. Wang, B.; Xing, W.; Zhao, Y.; Deng, X. Effects of chronic aluminum exposure on memory through multiple signal transduction pathways. *Environ. Toxicol. Pharmacol.* **2010**, *29*, 308–313.

[18]. Mergu, N.; Singh, A. K.; Gupta, V. K. Highly sensitive and selective colorimetric and off-on fluorescent reversible chemosensors for Al3+

based on the rhodamine fluorophore. *Sensors (Basel)* **2015**, *15*, 9097–9111.

[19]. Thangaraj, S. E.; Antony, E. J.; Selvan, G. T.; Selvakumar, P. M.; Enoch, I. V. M. V. A New Fluorenone-based Turn-on Fluorescent Al3+ Ion Sensor. *J Anal Chem* **2019**, *74*, 87–92.

[20]. Flaten, T. P. Aluminium as a risk factor in Alzheimer's disease, with emphasis on drinking water. *Brain Res. Bull.* **2001**, *55*, 187–196.

[21]. Barceló, J.; Poschenrieder, C. Fast root growth responses, root exudates, and internal detoxification as clues to the mechanisms of aluminium toxicity and resistance: a review. *Environ. Exp. Bot.* **2002**, *48*, 75–92.

[22]. Han, T.; Feng, X.; Tong, B.; Shi, J.; Chen, L.; Zhi, J.; Dong, Y. A novel "turn-on" fluorescent chemosensor for the selective detection of Al3+ based on aggregation-induced emission. *Chem. Commun. (Camb.)* **2012**, *48*, 416–418.

[23]. Jang, H. J.; Kang, J. H.; Yun, D.; Kim, C. A multifunctional selective "turn-on" fluorescent chemosensor for detection of Group IIIA ions Al3+, Ga3+ and In3+. *Photochem. Photobiol. Sci.* **2018**, *17*, 1247–1255.

[24]. Hirata, S.; Umezaki, Y.; Ikeda, M. Determination of chromium(III), titanium, vanadium, iron(III), and aluminum by inductively coupled plasma atomic emission spectrometry with an on-line preconcentrating ion-exchange column. *Anal. Chem.* **1986**, *58*, 2602–2606.

[25]. Joshi, P.; Painuli, R.; Kumar, D. Label-free colorimetric nanosensor for the selective on-site detection of aqueous Al3+. *ACS Sustain. Chem. Eng.* **2017**, *5*, 4552–4562.

[26]. Yu, F.; Hou, L. J.; Qin, L. Y.; Chao, J. B.; Wang, Y.; Jin, W. J. A new colorimetric and turn-on fluorescent chemosensor for Al 3+ in aqueous medium and its application in live-cell imaging. *J. Photochem. Photobiol. A Chem.* **2016**, *315*, 8–13.

[27]. Gui, S.; Huang, Y.; Hu, F.; Jin, Y.; Zhang, G.; Yan, L.; Zhang, D.; Zhao, R. Fluorescence turn-on chemosensor for highly selective and sensitive detection and bioimaging of Al(3+) in living cells based on ion-induced aggregation. *Anal. Chem.* **2015**, *87*, 1470–1474.

[28]. Komor, A. C.; Barton, J. K. The path for metal complexes to a DNA target. *Chem. Commun. (Camb.)* **2013**, *49*, 3617–3630.

[29]. Becke, A. D. Density-functional thermochemistry. III. The role of exact exchange. *J. Chem. Phys.* **1993**, *98*, 5648–5652.

[30]. Becke, A. D. Density-functional exchange-energy approximation with correct asymptotic behavior. *Phys. Rev. A Gen. Phys.* **1988**, *38*, 3098–3100.

[31]. Lee, C.; Yang, W.; Parr, R. G. Development of the Colle-Salvetti correlation-energy formula into a functional of the electron density. *Phys. Rev. B Condens. Matter.* **1988**, *37*, 785–789.

[32]. Frisch, M. J.; Trucks, G. W.; Schlegel, H. B.; Scuseria, G. E.; Robb, M. A.; Cheeseman, J. R.; Montgomery, J. A.; Vreven, T.; Kudin, K. N.; Burant, J. C.; Millam, J. M.; Iyengar, S. S.; Tomasi, J.; Barone, V.; Mennucci, B.; Cossi, M.; Scalmani, G.; Rega, N.; Petersson, G. A.; Nakatsuji, H.; Hada, M.; Ehara, M.; Toyota, K.; Fukuda, R.; Hasegawa, J.; Ishida, M.; Nakajima, T.; Honda, Y.; Kitao, O.; Nakai, H.; Klene, M.; Li, X.; Knox, J. E.; Hratchian, H. P.; Cross, J. B.; Adamo, C.; Jaramillo, J.; Gomperts, R.; Stratmann, R. E.; Yazyev, O.; Austin, A. J.; Cammi, R.; Pomelli, C.; Ochterski, J. W.; Ayala, P. Y.; Morokuma, K.; Voth, G. A.; Salvador, P.; Dannenberg, J. J.; Zakrzewski, V. G.; Dapprich, S.; Daniels, A. D.; Strain, M. C.; Farkas, O.; Malick, D. K.; Rabuck, A. D.; Raghavachari, K; Foresman, J. B.; Ortiz, J. V.; Cui, Q.; Baboul, A. G.; Clifford, S.; Cioslowski, J.; Stefanov, B. B.; Liu, G.; Liashenko, A.; Piskorz, P.; Komaromi, I.; Martin, R. L.; Fox, D. J.; Keith, T.; Al-Laham, M. A.; Peng, C. Y.; Nanayakkara, A.; Challacombe, M.; Gill, P. M. W.; Johnson, B.; Chen, W.; Wong, M. W.; Gonzalez, C.; Pople, J. A. Gaussian, Inc. , Wallingford CT, 2004.

[33]. Sheet, S. K.; Sen, B.; Thounaojam, R.; Aguan, K.; Khatua, S. Highly selective light-up Al3+ sensing by a coumarin based Schiff base probe: Subsequent phosphate sensing DNA binding and live cell imaging. *J. Photochem. Photobiol. A Chem.* **2017**, *332*, 101–111.

[34]. Chethan Prathap, K. N.; Lokanath, N. K. Three novel coumarin-benzenesulfonylhydrazide hybrids: Synthesis, characterization, crystal structure, Hirshfeld surface, DFT and NBO studies. *J. Mol. Struct.* **2018**, *1171*, 564–577.